An RF-Powered Wireless Temperature Sensor for Harsh Environment Monitoring With Non-Intermittent Operation

Parvaneh Saffari, *Student Member, IEEE*, Ali Basaligheh, *Student Member, IEEE*, Vincent J. Sieben, and Kambiz Moez, *Senior Member, IEEE*

***Abstract*—This paper presents a fully integrated RF-powered temperature sensor with non-intermittent operation. The sensor is powered up wirelessly from a 915-MHz incident signal using a power-efficient RF energy harvester, uses a subthreshold ring oscillator that produces a highly temperature-dependent oscillation frequency acting as a temperature-to-frequency converter, and finally transfers the frequency-modulated signal to an external reader using back scattering. The power management circuits are eliminated in the designed sensor to arrive at a minimalistic design. For proper operation, a novel voltage regulator is developed that produces a relatively constant output voltage as the supply voltage of the ring oscillator for a large range of harvested input energy but allows the output voltage to change as a function of the temperature for added temperature sensitivity of the overall sensor. Power consumption of the proposed sensor is only 1.05 μW at room temperature, which enables continuous operation of the sensor from an incident energy of −16 dBm. The sensor is tested between −10 °C to 100 °C exhibiting a minimum sensitivity of 238 Hz/°C at −10 °C and a maximum sensitivity of 31.648 kHz/°C at 100 °C. The predicted temperature error is −2.6 °C to 1.3 °C using a two-point calibration within the range of 10 °C to 100 °C. With a conversion time of 25 ms, 0.046 °C (rms) resolution is achieved. Fabricated in IBM's 130-nm CMOS technology, the proposed sensor occupies a die area of 0.23 mm^2.**

***Index Terms*—RF-powered wireless sensor, ring oscillator, voltage reference, voltage regulator, RF energy harvester.**

I. Introduction

RECENT progress in development of energy harvesting systems has opened the door to using ambient energy as an alternative to the energy stored in capacity-limited batteries for powering low-power wireless sensors and devices [1]. Recently the combination of power-efficient energy harvesting systems with low power CMOS sensory systems has extended the applications of CMOS sensors to wireless environmental or healthcare monitoring, especially thermal monitoring to monitor system reliability and performance as a function of temperature variation [2]–[7]. A radio frequency (RF) energy harvester produces a dc supply source by scavenging the electromagnetic energy either transmitted by a dedicated transmitting antenna or by other transmitters such as television/radio stations or cellular base stations. The harvested RF signal is sufficient for powering up a variety of low-power wireless portable electronic sensor and devices for many applications [8].

The major limitation of an RF energy harvesting system is the limited amount of the energy that can be scavenged from ambient electromagnetic waves or dedicated wireless power transmitters. The first reason for this is the reception of weak wireless signal whose power is limited by regulatory constraints on the maximum allowed transmitted power and fast attenuation of the signal power over distance [9]. The second reason is the relatively low power conversion efficiency of RF energy harvesters (RF-to-DC converter) that further reduces the power that can be scavenged. Therefore, to build a wireless sensor entirely powered by harvested RF energy, it is crucial to minimize the power consumption of sensor circuitry and wireless transmitter that is required to transmit the sensed data to a reader. To be able to power up a wireless sensor, one strategy is to allow for RF harvester to store enough energy in an on-board battery or capacitor and then wake up the sensor and transmitter circuitry for a limited time. This requires implementation of an active power management system that cycles between standby/charging mode and active mode [3]–[7], [10]. When enough energy accumulates during standby mode, the whole system turns ON in active mode. These structures need a power management unit or a mode selector to monitor the storage power and select between these two modes. However, these power management units increase the complexity of the circuit and consume additional power. Furthermore, the toggling between charge and active modes means that these circuits do not work continuously as no data is measured or transmitted in their standby mode. If the circuit to be powered by the RF energy harvester consumes less power than the total harvested power, the sensor can operate continuously. This removes the need for a power management unit and also decreases the complexity and size of the device.

Manuscript received May 30, 2017; revised August 22, 2017 and September 19, 2017; accepted September 21, 2017. Date of publication October 11, 2017; date of current version April 2, 2018. This work was supported by the Natural Sciences and Engineering Research Council of Canada. This paper was recommended by Associate Editor Z. Tan. *(Corresponding author: Parvaneh Saffari.)*

P. Saffari, A. Basaligheh, and K. Moez are with the Department of Electrical and Computer Engineering, Faculty of Engineering, University of Alberta, Edmonton, AB T6G2V4, Canada (e-mail: saffari@ualberta.ca; kambiz@ualberta.ca).

V. J. Sieben is with the Schlumberger-Doll Research, Cambridge, MA 02139 USA.

Color versions of one or more of the figures in this paper are available online at http://ieeexplore.ieee.org.

Digital Object Identifier 10.1109/TCSI.2017.2758327

In this paper, an ultra-low power, RF-powered wireless temperature sensor with continuous operation is presented. The sensor is developed to monitor the temperature inside a high-pressure high-temperature chamber to eliminate the costly bulkhead connection to such a chamber. To power the wireless sensor solely by harvested RF energy, a minimalistic design approach is adopted to minimize the number of sensor's building blocks that are required to harvest the RF energy, sense the temperature, and transmit the sensor data wirelessly to an external reader. Also, each building block must consume the minimum power that is needed to adequately perform its function. One approach for reducing power consumption is the use of subthreshold circuits, which are becoming increasingly popular in low-power, low-voltage designs [11]. Subthreshold operation can be achieved by scaling down the power supply below the threshold voltage [12], [13]. A ring oscillator operating in subthreshold region is used for temperature sensing not only because its low power consumption but also because its oscillation frequency varies exponentially with temperature [14]. To power up the ring oscillator from harvested RF energy, a new supply voltage regulator is designed that produces an output voltage which remains relatively constant for a large input voltage range but changes as a function of temperature adding to the temperature sensitivity of the ring oscillator and improving the exponential behavior of the oscillator's output frequency as a function of temperature. In order to use a single antenna (coil) for both energy harvesting and wireless data transmission avoiding the use of duplexers, a backscattering technique is employed that reflects back a significant portion of incoming RF energy with a frequency that is the function of the sensed temperature.

The wireless sensor presented in this paper is designed and implemented in a standard 130 nm CMOS technology. The paper is organized as follows: Section II describe the existing RF-powered wireless sensors in details proving the background necessary to understand the proposed sensor architecture. Section III describes the proposed system architecture where building blocks of the system are explained in the subsections; Section IV reports the measurement results; finally, Section V concludes the paper.

II. Existing RF-Powered Wireless Sensors

There are several reports of RF-powered wireless sensors [2]–[7], [15]–[17]. In [3], a wireless temperature sensor is presented that utilizes a half wave rectifier producing dc supply voltage for the other system blocks. A mode selector circuit that is based on a hysteresis comparator decides whether the system is in standby mode or active mode. When the circuit is in active mode a bootstrapped voltage source temperature sensor generates a complementary to absolute temperature (CTAT) voltage. The CTAT voltage sets the voltage control on MOS varactors of a cross coupled oscillator to modulate the output frequency with changes in ambient temperature. The sensed data is transmitted by a class AB power amplifier. In [17], a RF identification (RFID) sensor for human body temperature monitoring is presented. In this paper a differential voltage multiplier with Schottky diodes is implemented to provide required energy for the other blocks. Two voltage regulators are implemented. One of them supplies a regulated voltage to digital core and the other one supplies a regulated voltage to the analog part. The digital core controls the communication flow with the reader. In this paper a bootstrapped current source generates a temperature-dependent supply current. This temperature-dependent current provides the supply current for a ring oscillator. As far as the supply current of the ring oscillator varies with temperature, the output frequency varies with temperature in a proportional way. A 15-bit binary counter counts the number of pulses delivered by the oscillator in a fixed time interval. In [7] an RF-powered temperature sensor for biomedical applications is presented. A mode selector monitors the supply voltage and enables the other blocks when rectifier collects enough energy in charging mode. A voltage regulator is used in this system for providing the stable voltage. A threshold based current reference generator is employed as a temperature sensor in this work. A current starved ring oscillator modulate the output frequency based on the temperature-dependent current of the sensor. Data is sent back to outside through current starved ring oscillator and a back scattering switch.

As discussed, most of existing RF-powered wireless sensors use power management systems to activate the sensor circuitry when the enough energy is accumulated during the standby mode. Also, most of the reported RF-powered wireless temperature sensors have a voltage sensor to generate a temperature dependent voltage/current and a temperature-independent oscillator to modulate the output frequency or pulse width based on the measured sensor temperature, thus requiring two essential blocks for sensing and wireless transmission. Cross-coupled LC tank oscillators are often used to produce a temperature-independent voltage-independent oscillation frequency but these kinds of oscillators are consuming large current to be able to provide the oscillation conditions [3], [15]. Another method of generating temperature and voltage independent oscillation is using low power oscillators such as current starved ring oscillators that modulate the output frequency based on the temperature-dependent current of the sensor [7], [17]. However these kind of oscillators are voltage dependent, thus a voltage regulator is needed. In this case, the added power consumption of the voltage regulator must be considered.

To achieve a minimalistic design for an RF-powered wireless sensor with ultra-low-power consumption, we have taken the following initiatives. First, for reducing the power consumption and chip area, we have combined the sensor circuitry and oscillator part by using a subthreshold ring oscillator temperature sensor both for sensing the temperature and modulating the wireless signal. This will produce a temperature-dependent frequency modulated signal that can be transmitted to the reader. However, as the oscillation frequency of the subthreshold ring oscillator varies not only as a function of the temperature but also as a function of supply voltage (V_{DD}). For producing an oscillation frequency that is independent of variation in supply voltage caused by varying incoming signal power, a very low-power subthreshold voltage regulator with embedded voltage reference is designed that produces a

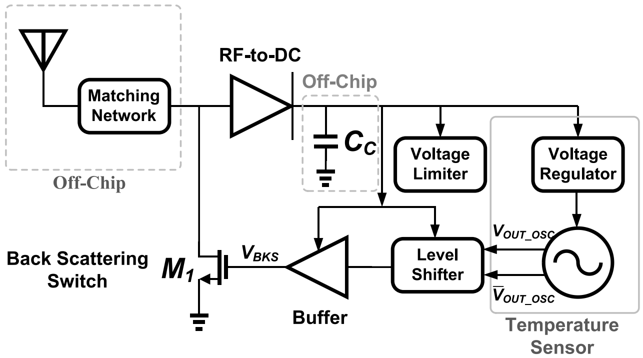

Fig. 1. Block diagram of proposed RF-powered wireless sensor.

supply voltage that is relatively constant for a wide range input voltages but varies with temperature resulting added sensitivity of the temperature sensor circuit. Second, to reduce the overall sensor power consumption and complexity, we have eliminated the power management circuitry that is required for wake-up sensing and transmission operation (intermittent operation). To achieve this goal, the desired sensor is designed with such low power consumption that is less than the total harvested power for continuous operation.

III. Proposed RF-Powered Wireless Sensor

A block diagram of the proposed RF-powered wireless sensor is presented in Fig. 1. An antenna (or coil) collects the incident RF signal from the dedicated wireless power transmitter or ambient electromagnetic energy. A matching network is required to enable maximum power transfer from antenna to RF-DC power converter. The high efficiency RF-DC converter converts the incident RF power to dc voltage. The dc voltage is stored in an external large capacitor C_c acting as a dc supply voltage for powering the other circuitries in the system.

A voltage limiter is placed directly after the rectifier output to limit the voltage to the highest supply voltage supported by this technology, which is 1.5 V as per IBM's 130 nm CMOS technology, to avoid voltage breakdown of transistors. As the output voltage of RF-to-DC rectifier varies with the amount of received RF energy and power consumption of the circuitry powered by the rectifier, a voltage regulator is needed to produce a stable output voltage for biasing the rest of the system in subthreshold region. The proposed voltage regulator is designed in a way to produce stable output voltage for a wide range of input voltage generated by variable received RF energy but allows the output voltage to increase with temperature that can be used to increase the temperature sensitivity of the sensor. The next block is the ring oscillator temperature sensor. The ring oscillator is biased in the subthreshold region and has high dependency to temperature [14]. By biasing the ring oscillator in the subthreshold not only the power consumption is reduced substantially but also the oscillation frequency of the ring oscillator become stronger function of temperature compared to a regular ring oscillator. Upon a change in temperature, both the output voltage of the regulator and the ring oscillator frequency sensitivity yield a combined shift of the characteristic frequency in the same direction.

A level shifter is attached to the output of the ring oscillator. Biasing the ring oscillator at subthreshold results in a low output's amplitude, which is not able to actuate the ON-OFF back scattering switch. A simple level shifter is used to shift the output of the ring oscillator to the V_{DD} (output of the rectifier) without altering the frequency.

The level shifter output is applied to the back scattering switch. When the output of the level shifter is high, the back scattering switch is ON and it is conducting current. Its low ON resistance ($Z_{in} \sim 0$) creates a strong mismatch at the output of antenna causing most of the signal power reflected back to the reader. When the back scattering switch is OFF as the input impedance of the rectifier is matched to the output impedance of the antenna, little power will be reflected by the antenna. As the output frequency of the ring oscillator is a function of sensed temperature, the ON-OFF switching frequency of the back scattering switch that can be detected by an external reader by observing the reflected signal strengths on the transmitting antenna can be used for sensing the temperature sensed by the wireless sensor.

A. RF to DC Converter

The RF-to-DC power converter extracts the required dc power for powering up the rest of the system. Sensitivity and power conversion efficiency (PCE) of the rectifier are the most important factors that could affect the operating range of the sensor and required minimum power transmission from the antenna. The performance parameters of RF-DC converters such as PCE are mostly affected by the threshold voltage of the rectifying devices. Several works have been reported on the compensation of threshold voltages of the rectifying devices [18]–[22]. Although static threshold voltage compensation improves the forward bias performance of the rectifying device but increase the reverse bias leakage as well, degrading the efficiency performance [23]. There are recent works in RF energy harvesting that incorporate power management with ultra-low power consumption [24]–[26].

In this paper for simplicity a PMOS 10-stage with Dickson topology [27] is designed to provide 800 mV output voltage at room temperature from minimum input incident power of -16dBm that is required for proper operation of the downstream voltage regulator. The advantage of PMOS in comparison to NMOS is that PMOS's bulk can be connected to its source that prevents increasing threshold voltage of later stages because of the body effect [22]. A block diagram of the complete rectifier along with the schematic of a single stage are given in Fig. 2. The coupling capacitors C1 and C2 in this design are chosen as 4pF.

B. Voltage Limiter

For IBM's 130 nm CMOS process, the maximum allowed supply voltage for avoiding breakdown is 1.5 V. The voltage limiter is designed to sink a large current when the input voltage exceeds 1.5 V. the designed voltage limiter is shown in Fig. 3. When the output voltage of the rectifier exceeds 1.5 V current starts to flow from resistor R_2, makes the gate voltage of PMOS transistor M_2 low enough to turn it on and in

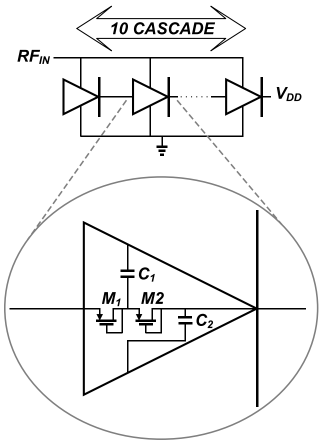

Fig. 2. Block diagram of the RF-DC converter.

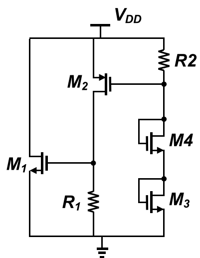

Fig. 3. Voltage limiter schematic.

turn switches the NMOS transistor M_1 on which flows most of the current [28]. Therefore, the dc voltage output produced by the rectifier is limited to a maximum of 1.5V and guarantees reliable operation of system.

C. Voltage Regulator and Voltage Reference

As the output voltage of RF-to-DC rectifier varies with the amount of received RF energy and power consumption of the circuitry powered by the rectifier, a voltage regulator is needed to produce a stable output voltage for biasing the rest of the system in subthreshold region. As will be discussed in the next section, the temperature sensor used in our design is a ring oscillator which its output frequency is a strong function of its supply voltage. Therefore, variation of output voltage produced by the rectifier cannot be neglected. It is important to note that the most regulators are designed in a way to stabilize the output voltage versus varying input voltage and ambient temperature changes [11], [29], [30]. Our voltage regulator is designed to stabilize the voltage against the input voltage variation, but not against temperature variation. The regulator's output voltage varies with temperature in the same direction as the frequency of the ring oscillator. As temperature goes up, the output voltage of the regulator also increases. The output voltage of the regulator is used to power the next stage, which is the ring oscillator temperature sensor. The temperature-dependency of the regulator's output voltage not only increases the sensitivity of the sensor but also helps to produce a purely exponential relation between the frequency and temperature of the ring oscillator as will be further discussed in Section III. D.

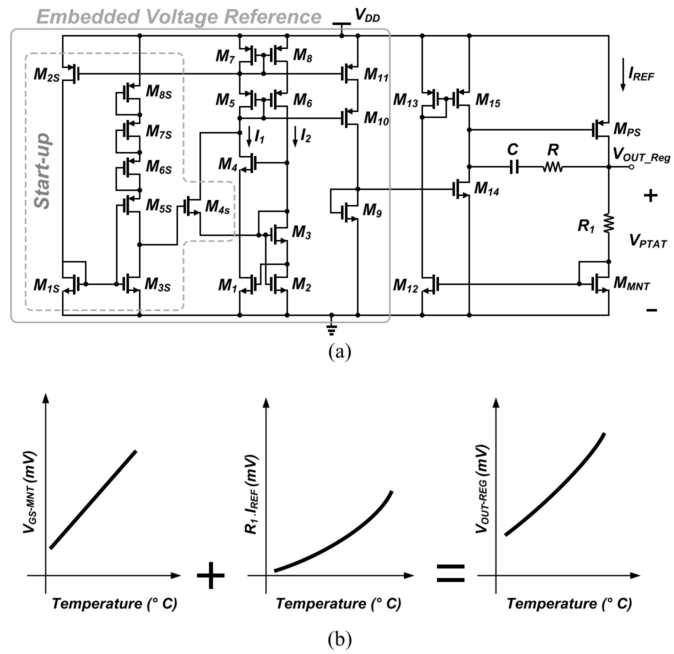

Fig. 4. (a) Designed voltage regulator with embedded voltage reference, (b) Behavioral drawing of V_{GS-MNT}, $R_1 I_{REF}$ and V_{OUT_Reg}.

Chen *et al.* [29], presented a sub-1V voltage regulator with embedded voltage reference. In [29], a reference current is produced that is independent of the MOSFETs's characteristics and supply voltage. In our design, because of channel length modulation effect in the CMOS process that we use for implementation of the sensor, the voltage reference presented in [11] with minor modifications is used instead of the current reference implemented in [29] to achieve a less dependent output voltage than the one produced by [29]. The designed voltage regulator with embedded voltage reference is shown in Fig. 4(a).

All the transistors except M_{PS} are designed in subthreshold region that ensure low power consumption. To find the relation between the regulator's output voltage and temperature, we start by writing the transistor current in the subthreshold region, $i_{D,Sub}$, as [31]

$$i_{D,sub} = \mu_{eff} C_{OX} \frac{W_{eff}}{L_{eff}} (m-1) (\frac{k_B T}{q})^2 \times \exp(\frac{q}{m k_B T}(V_{GS} - V_{TH})) \times (1 - \exp(-\frac{q V_{DS}}{k_B T})), \quad (1)$$

where μ_{eff} is the effective mobility of carriers in the channel, C_{ox} is the gate oxide capacitance per unit area, W_{eff} and L_{eff} are the effective channel width and length of transistor respectively, m is the subthreshold slope factor, and k_B is Boltzmann constant that is temperature independent, ,and V_{DS} is the drain-source voltage of the transistor. For $V_{DS} \gg k_B T/q$, Equation (1) simplifies to

$$i_{D,sub} = \mu_{eff} C_{OX} \frac{W_{eff}}{L_{eff}} (m-1) (\frac{k_B T}{q})^2 \times \exp(\frac{q}{m k_B T}(V_{GS} - V_{TH})), \quad (2)$$

where temperature-dependency of the carrier mobility and threshold voltage can be described by the following relations [32]:

$$\mu_{eff} = \mu_0 \left(\frac{T}{T_0}\right)^{-1.5} \text{ and } V_{TH} = V_{TH0} + \alpha_{V_{TH}}(T - T_0), \tag{3}$$

where V_{TH0} and μ_0 are the threshold voltage and carrier mobility at $T=T_0^{\circ}K$, and α_{VTH} is the threshold voltage coefficient that is negative.

Writing KVL for the loop created by gate-source terminal of transistors M1, M2 and M3, we can find that $V_{GS2}=V_{GS1} + V_{GS3}$. Knowing these transistors are biased at subthreshold region and using the I_1 is mirrored to I_2 by a factor of $\alpha(I_2=\alpha I_1)$, the drain current of M_1 can be calculated as

$$I_1 = A\mu_{eff}C_{OX}(m-1)\left(\frac{k_B T}{q}\right)^2 \exp\left(-\frac{\Delta V_{TH}}{\frac{k_B T}{q}m}\right), \tag{4}$$

where $A = (W/L)_1(W/L)_2/(W/L)_3$ and $\Delta V_{TH} = V_{TH1} + V_{TH3} - V_{TH2}$ [11]. The output voltage of regulator ($V_{OUT-Reg}$) is equal to $V_{GS\_MNT} + R_1 I_{REF}$ based on KVL at the regulator output. I_{REF} is proportional to I_1 that is determined by the voltage reference part. Thus $V_{OUT-Reg}=V_{GS}\_MNT+K.R_1.I_1$, where K is independent of temperature and it is proportional to the sizes of transistors M_7, M_9, M_{11--15} and M_{NT}. From (2) V_{GS_MNT} can be expressed as

$$V_{GS\_MNT} = V_{TH\_MNT} - \Delta V_{TH} + m\frac{k_B T}{q}\ln\left(\frac{A.K}{\left(\frac{W}{L}\right)_{MNT}}\right). \tag{5}$$

V_{TH_MNT} is complementary to absolute temperature (CTAT) but $-\Delta V_{TH}$ and the last term in (5) is proportional to absolute temperature (PTAT). By proper sizing of transistors, coefficient $A.K$ will be large enough that V_{GS_MNT} has a PTAT coefficient. As all the terms in (5) are linearly dependent to temperature, V_{GS_MNT} is linearly increasing with temperature. The other term in V_{OUT_Reg} expression is $K.R_1.I_1$ which has a PTAT coefficient as well but it is not linearly proportional to temperature because of nonlinear relation of I_1 and temperature (proven in Equation (4)) although resistor R_1 has a linear dependency on temperature. Therefore $V_{OUT-Reg}$ is PTAT as it is the sum of two terms, V_{GS_MNT} and $K.R_1.I_1$, with PTAT coefficients. The temperature dependencies of V_{GS_MNT}, $K.R_1.I_1$ and V_{OUT_Reg} are shown in Fig 4(b). As will be discussed in section III.D, ring oscillator's output frequency versus temperature is not completely exponential with a supply voltage (V_{OUT_Reg}) that is linearly increasing with temperature. By adding the nonlinear term of $K.R_1.I_1$ in V_{OUT_Reg}, V_{OUT_Reg} is designed to become such a nonlinear function of temperature to produce an exponential relation between the ring oscillator frequency and temperature when its supply voltage connected to the output of the devised voltage regulator.

The output voltage of the designed regulator is 165mV at room temperature. The low output voltage of the voltage regulator guarantees the subthreshold operation of the ring oscillator temperature sensor.

D. Temperature Sensor

A ring oscillator biased in subthreshold region has a high sensitivity to temperature and consumes limited power [14]. The current of transistor biased in subthreshold region is exponentially dependent on the temperature, thus ring oscillators operating in subthreshold region can be used for construction of a temperature sensor with high sensitivity [14]. Hence as temperature increases, the frequency of ring oscillator increases as delays of the loop inverters decreases.

In this sensor, frequency increases both with increasing temperature and power supply voltage. The oscillation frequency (*Freq*) of a ring oscillator is inversely proportional to the time delay (t_d) of the inverter which in turn is proportional to the average ON current of the inverter (i_D) and inversely proportional to the total output capacitance of each stage (C_o) and the output voltage swing of ring oscillator (V_H-V_L) as described by the following equation [14]:

$$Freq = \frac{1}{t_d} \approx \frac{i_D}{C_o(V_H - V_L)}. \tag{6}$$

In our design, the inverters are working in subthresold region, where i_D in subthreshold region is given by (2).

The temperature coefficient of i_D can be expressed as

$$\begin{aligned} TCC_{sub} = \frac{1}{i_D}\frac{di_D}{dT} &= \frac{1}{\mu_{eff}}\frac{d\mu_{eff}}{dT} \\ &+ \frac{2}{T} + \frac{q}{mk_BT}\frac{dV_{GS}}{dT} - \frac{q}{mk_BT}\frac{dV_{TH}}{dT} \\ &- \frac{1}{T}\ln\left(\frac{i_{D,sub}L_{eff}}{W_{eff}\mu_{eff}C_{OX}(m-1)}\left(\frac{q}{k_BT}\right)^2\right). \end{aligned} \tag{7}$$

Based on (3), μ_{eff} and threshold voltage V_{TH} are temperature dependent and determine *TCC* [14], [33]. Both V_{TH} and μ_{eff} are inversely proportional to temperature, but the variation of V_{TH} is dominant. By increase of temperature, μ_{eff} attenuates the current but V_{TH} intensifies the current. Since the effect of V_{TH} is dominant, the total change in current increases by increasing the temperature. Equation (7) clearly shows that *TCC* of the transistor's current in the subthreshold region is a function of the gate-source voltage (V_{GS}). As the transistor's current is an exponential function of V_{GS}, the transistor's current exponentially increases with V_{GS}. On the other hand as it can be seen in Equation (6), the oscillation frequency is reduced by increasing output voltage swing (or V_{GS}). However, the exponential dependency to V_{GS} dominates resulting in increased oscillation frequency with increasing V_{GS}. Therefore, if the gate-source voltage proportionally increases with temperature, t_d is further reduced and frequency of the ring oscillator is further increased with temperature compared to the case where the gate-source voltage is kept constant with temperature. Consequently, the sensitivity of the oscillation frequency of the ring oscillators will increase if the supply voltage itself is an increasing function of temperature.

Output of the regulator plays the role of power supply for temperature sensor. As discussed in the last part, the regulator is designed in a way that its output voltage is directly porportioanl to temperature. Thus as the temperature increases, frequency increases because of two factors: first, increasing the power supply as regulator produce an output voltage that

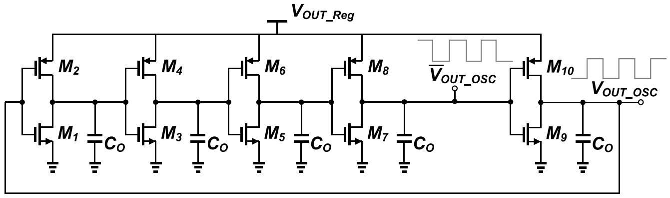

(a)

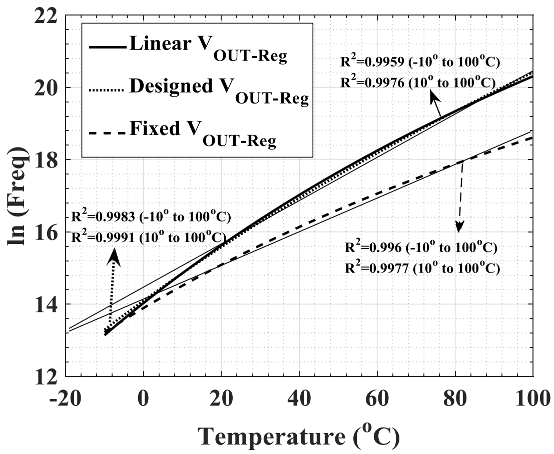

(b)

Fig. 5. (a) Schematic of the temperature sensor ring oscillator. (b) ln (Freq) versus temperature (Analytical result).

increases with the temprature, and second, inherent property of a subthreshold region oscillator that its output frequency increases by temperature. Thus this structure has an enhanced sensitivity to temperature. Schematic of the ring oscillator temperature sensor is shown in Fig. 5(a). In ring oscillators the output of inverters in each stage swings between the supply voltage (in our case V_{OUT_Reg}) and *GND* periodically. Output of each inverter is connected to the gate of NMOS of the next inverter thus the V_{GS} of the NMOS transistors in ring oscillator structure also varies periodically from V_{OUT_Reg} to *GND*. While the relation between the output frequency of subthreshold ring oscillator with constant supply voltage is examined in [34], here we need to find the behavior of the output frequency with respect to temperature for a ring oscillator with variable supply voltage. Assuming the supply voltage linearity increases with temperature, the gate-source voltage of the transistor can be written as:

$$V_{GS} = V_{OUT\_Reg} = V_{OUT\_Reg0} + \alpha_{V_{OUT\_Reg}} T. \tag{8}$$

By substituting (3) and (8) in (2), $i_{D,sub}$ can be rewritten as

$$i_{D,sub} = \alpha_1 T^{0.5} \exp(\frac{\alpha_2}{T}(\alpha_3 + T)), \tag{9}$$

where

$$\alpha_1 = \mu_0 T_0^{1.5} C_{ox} \frac{W_{eff}}{L_{eff}}(m-1)(\frac{k_B}{q})^2, \tag{10}$$

$$\alpha_2 = \frac{q(\alpha_{V_{OUT\_Reg}} - \alpha_{V_{TH}})}{m k_B}, \tag{11}$$

and

$$\alpha_3 = \frac{V_{OUT\_Reg0} - V_{TH0}}{\alpha_{V_{OUT\_Reg}} - \alpha_{V_{TH}}}. \tag{12}$$

As explained the output swing of ring oscillator is equal to V_{OUT_Reg}. Thus (6) can be rewritten as

$$Freq \approx \frac{i_{D,sub}}{C_o V_{OUT\_Reg}}, \tag{13}$$

where $i_{D,sub}$ and V_{OUT_Reg} are given in (9) and (8), respectively. Taking the natural logarithm (*ln*) of both sides in (13) gives us

$$\ln(Freq) = \ln(\alpha_1) + \frac{1}{2}\ln(T) + \alpha_2 + \frac{\alpha_2\alpha_3}{T} - \ln(C_o) - \ln(V_{OUT\_Reg0} + \alpha_{V_{OUT\_Reg}} T). \tag{14}$$

For selected values of ($\mu_{eff}C_{ox}W_{eff}/L_{eff}$=688.2$\mu A/V^2$, *m=1.4*, C_O=354fF, V_{TH0}=476mV, α_{VTH}=-0.8mV/°C, $T_0 = 0$ °C, V_{OUT_Reg0}=140mV, α_{VOUT_Reg}=0.957mV/°C), *ln (Freq)* is plotted in Fig. 5(b) based on (14). $\mu_{eff}C_{ox}W_{eff}/L_{eff}$, m, C_O, V_{TH0}, α_{VTH} are estimated from simulations of NMOS transistor in 130nm CMOS and V_{OUT_Reg0} and α_{VOUT_Reg} are approximated from linear fitting of measurement results of voltage regulator as will be shown in Section IV. As can be seen in Fig. 5(b), R^2 correlation between the linear fit and calculated ln (Freq) for a linear-varying V_{OUT_Reg} is 0.9959 for the temperature range of −10°C to 100°C and is 0.9976 for the temperature range of 10°C to 100°C. As discussed in Section III.C, we intentionally made the voltage regulator nonlinear to make the logarithm of ring oscillator's output frequency more linear. The ln (Freq) versus temperature for the designed voltage regulator is depicted in Fig. 5(b) where V_{OUT_Reg} is the same as the measurement output voltage of the regulator as shown in Fig. 11. The R^2 correlation in this case has improved to 0.9983 for the temperature range of −10°C to 100°C and to 0.9991 for the temperature range of 10°C to 100°C. Therefore, the designed voltage regulator's output voltage helps make the behavior of ln (Freq) of ring oscillator a more linear function of temperature. Comparing the correlation factors of the oscillator's output frequency for the fixed, the linear, and the designed supply voltage as shown in Fig. 5(b), it can be concluded that the designed voltage regulator not only increase the sensitivity but also improve the exponential behavior of the oscillator's output frequency as a function of temperature. As such, we can apply a two-point calibration on logarithm of frequency for calibrating the proposed sensor.

E. Level Shifter and Buffer

As the ring oscillator temperature sensor is biased in the subthreshold region, the peak output voltage amplitude is not sufficient to be able to turn on the back scattering switch. Level shifter shifts output voltage of the ring oscillator to the highest dc available voltage in the circuit, which is V_{DD}, the output voltage of the RF-DC converter. For low power consumption and high temperature sensitivity, the output voltage of the regulator is designed to be 165mV. Thus a level shifter that is very sensitive to low voltages is required to be able to sense very low voltage variations properly and shift it up to V_{DD}. The level shifter that is used in this circuit is based on [35]. Fig. 6 shows the schematic of the level shifter. After the level

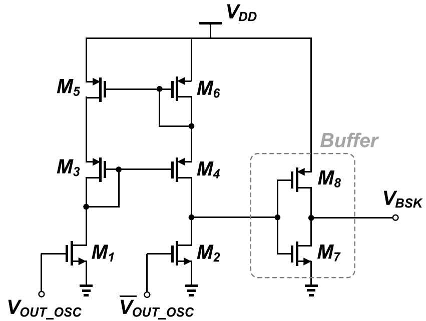

Fig. 6. Level shifter and buffer.

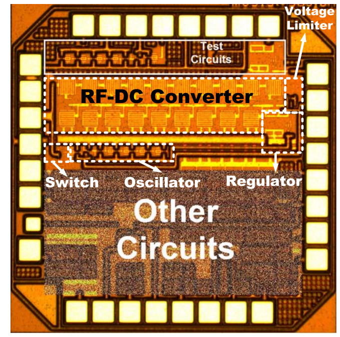

Fig. 7. Chip microphotograph.

shifter, a one stage buffer is used to isolate the level shifter from the back scattering switch. The level shifter and buffer do not change the frequency of the temperature sensor. The output frequency of the level shifter and buffer is the same as the frequency of the ring oscillator.

F. Backscattering

Backscattering is performed by an NMOS switch, responsible for sending the information to the reader. Output of the buffer is applied to the backscattering switch turning ON the backscattering switch when the output of the buffer is high, and turning it OFF when the output of the buffer is low. By switching between ON-OFF, the input impedance is changed. When the switch is OFF, the input is matched as $Z_{in} = 50$ ohm, and there is no reflection. When the switch is ON, it is conducting current and Z_{in} is mismatched. Therefore, a significant portion of the incident signal is reflected back to the reader. The reflected signal strength will change periodically with a frequency that is equal to the frequency of buffer output driven by the temperature sensing ring oscillator. As the sensed data is transmitted by a backscattered signal produced by modulating the incident signal, at no time of the operation the RF power source can be turned off. If there is no RF power source at any given time, no signal will be backscattered to reader and no erroneous temperature reading will occur due to the interruption in wireless powering.

G. Matching Network

Impedance matching circuit is crucial for optimizing the performance of the RF energy harvesting system. An impedance matching circuit is required to maximize power transfer between the source and the circuit when the backscattering switch is OFF. The impedances of the source and the load are matched at the desired operating frequency such that the impedances are complex conjugates of each other. To allow maximum power transfer, the input impedance of the circuit should be matched to 50 ohms. An off-chip L-section impedance input matching network is implemented on a printed circuit board using off-chip components. This matching network consists of a parallel inductor with a series capacitor. Discrete inductor from MURATA-LQW18AN series with quality factor of more than 80 and discrete capacitor from AVX-Accu-P series with quality factor of more than 200 are chosen for the matching network to minimize the insertion loss and maximize the sensitivity.

IV. Experimental Results

Fig. 7 shows the chip microphotograph of the fabricated wireless sensor, occupying a small core area of 0.23 mm^2 (without the charging capacitor and matching network) implemented using IBM's 130nm process with eight layers of metallization. Electrostatic discharge (ESD) protection is used on all pads. The die is packaged in a 36-pin QFN package. The chip is soldered onto a 2-layer FR-4 PCB board and tested with Agilent 8648D signal generator in the 902–928 MHz industrial, scientific and medical (ISM) band.

A. Testing of Individual Building Blocks

Before testing the overall sensor performance, each individual block is tested to ensure its functionality and show adequate performance as detailed below.

The RF-to-DC converter was tested by connecting an off-chip capacitor to the output as the energy storage component. Fig. 8(a) and Fig. 8(b) show the measured output voltage of the rectifier and voltage regulator at room temperature when RF-to-DC converter is driven with a −16 dBm input power and is loaded with the other circuits of the wireless sensor with storage capacitors of 1 μF and 100 pF. The comparison between the Fig. 8 (a) and Fig. 8 (b) shows that when the capacitor is 1 uF, the rise time of RF-DC converter is 320 ms but with lower ripples. When the storage capacitor is reduced by a factor of 10 to 100 pF, the rise time of RF-DC converter is reduced by a factor of 10 to 33 ms as well but the ripples are increased as expected. As the output of RF-DC is regulated by voltage regulator, these ripples are suppressed by voltage regulator as shown in Fig. 8 (b). Therefore, the sensor can work with a wide range of the storage capacitor (tested 100 pF- 1 uF) as long as the ripple caused by small capacitors can be filtered by the regulator and the long rise time caused by large capacitors can meet the sensor's required wake-up time specifications.

Fig. 8(c) shows the simulated PCE with and without activated switch when the rectifier is connected to 1MΩ load and the estimated measured PCE of the designed RF-to-DC converter when is loaded with wireless sensor and activated

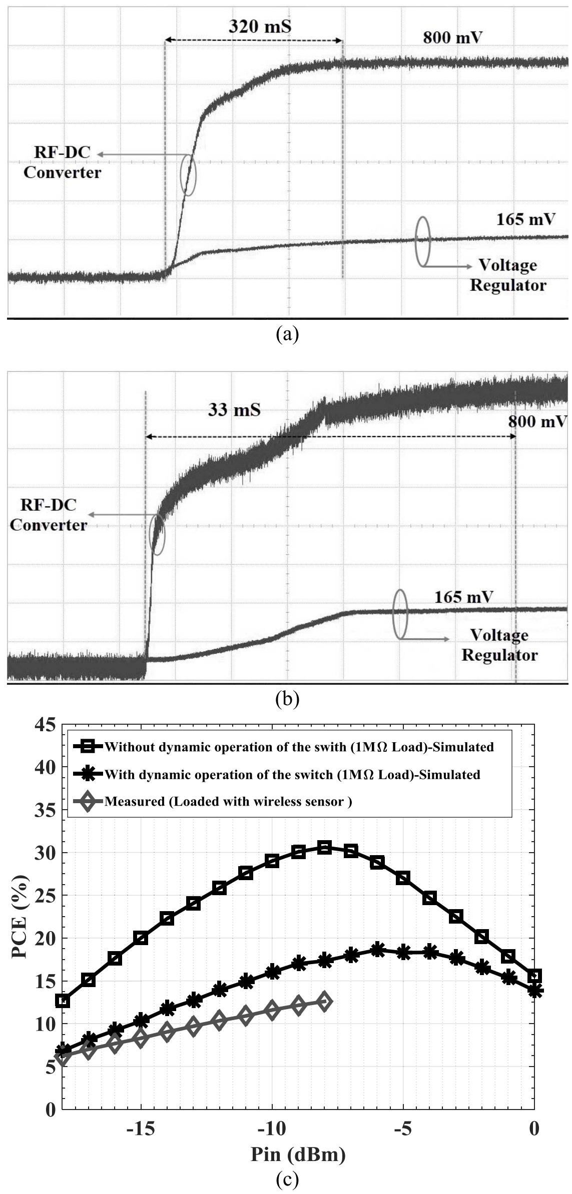

Fig. 8. (a) Measured output voltage of RF-DC converter and voltage regulator versus time for C_c of 1 uF, (b) measured output voltage of RF-DC converter and voltage regulator versus time for C_c of 100 pF, and (c) simulated PCE with and without dynamic operation of switch with 1 MΩ load and measured PCE when the harvester is loaded with wireless sensor during the dynamic operation of the switch.

backscattering switch. The simulated power conversion efficiency of the rectifier is 17.63% when the input power of −16 dBm is applied directly to the rectifier and the rectifier is connected to 1MΩ load and the backscattering switch is not activated. The estimated measured PCE of the designed RF-to- DC converter when is loaded with wireless sensor and activated backscattering switch at the input power of −16 dBm is 7.67%. To increase the scavenged power, the proposed system can be designed with much lower backscattering duty cycle than the current 50%, allowing the RF-to-DC converter to harvest RF energy for the most of the duty cycle while backscattering a signal with same frequency modulation.

In order to verify the functionality of the voltage limiter in simulation the supply voltage of the voltage limiter is swept

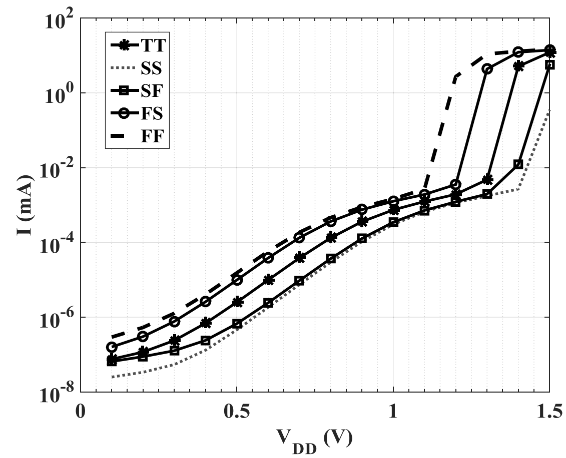

Fig. 9. Limiter's simulated current consumption across the corners.

between 0 and 1.5V, while the current dissipated in the voltage limiter is monitored. The simulated data is available in Fig. 9. It can be seen from the simulation results that after a voltage, voltage limiter sinks tens of milliamps to amps and that will protect other parts. The dependency of voltage limiter to process variation is not an issue. The desired operation voltage of the designed temperature sensor network is around 800 mV. For different process corners, as can be seen in Fig. (9) the rail voltage will be limited to 1.1 V for fast-fast (FF) corner to 1.4 V for slow-slow (SS) corner. This is well within the reliable operation voltage range of CMOS technology used in design of the sensor as transistors will reliably operate with voltages less than 1.5 V in 130 nm CMOS. As part of the system, the functionality of the voltage limiter is verified by monitoring the output voltage of the RF-to-DC converter that did not exceed 1.2 V by increasing input power range.

To test the voltage regulator the voltage on the charging capacitor was swept between 0 to 1.2V for different temperatures from −10° to 100°, while the output voltage of the voltage regulator is measured by a digital multimeter, the measured data is available in Fig. 10. and Fig. 11. It can be seen from the measurement result that for each single temperature output voltage of the regulator is stable by variation of input voltage. As temperature increases voltage regulator's output voltage increases.

B. Testing of Overall Sensor

The measurement setup for direct and wireless powering is shown in Fig. 12.

To verify the proper operation of the sensor, we first started by connecting the input power directly to the RF power generator through a 50 Ohm coaxial cable and monitoring the input terminal voltage. The backscattering switch turns on/off with the output frequency of the ring oscillator that is indicative of the sensed temperature. To measure the temperature sensitivity, the device is put in the temperature chamber. The sensor is powered up directly with the signal generator and output waveform is obtained with the oscilloscope. The resolution of temperature chamber was 0.1°C over a temperature range of −10°C to 100°C.

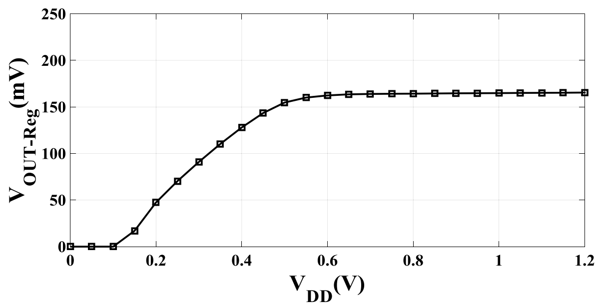

Fig. 10. Measured output voltage of voltage regulator as a function of RF-DC converter's (V_{DD}) output at room temperature.

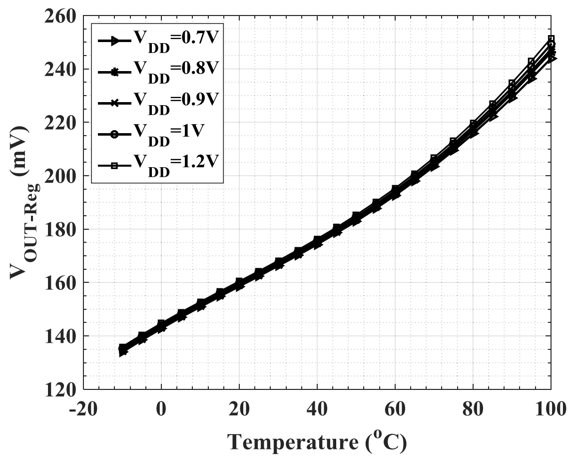

Fig. 11. Measured temperature dependence of the regulated voltage for different supply voltages.

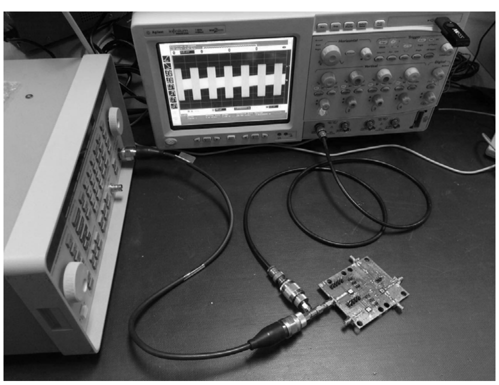

(a)

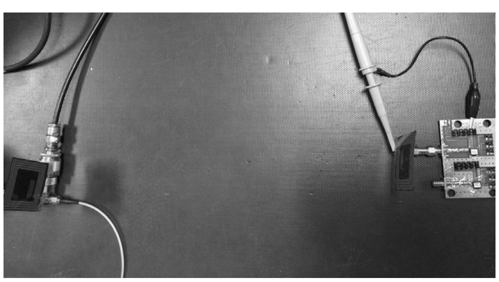

(b)

Fig. 12. (a) Measurement setup for direct powering. (b) Measurement setup for wireless powering.

Fig. 13 shows the reflected voltage waveform of chip 1 for 35°C, 52°C and 70°C when the sensor is powered directly with −16 dBm input power. The reflected voltage waveforms

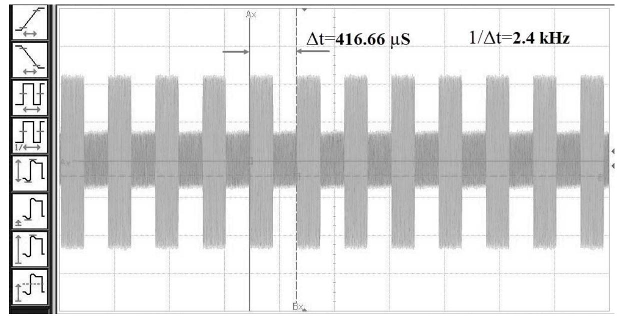

(a)

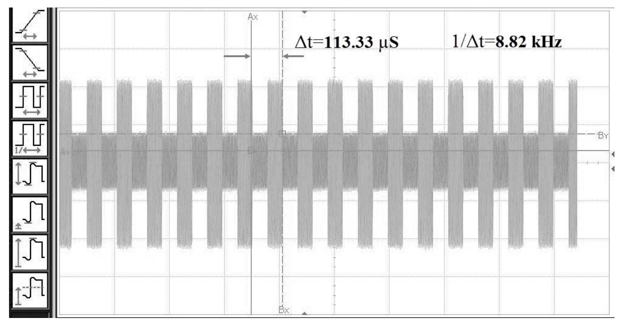

(b)

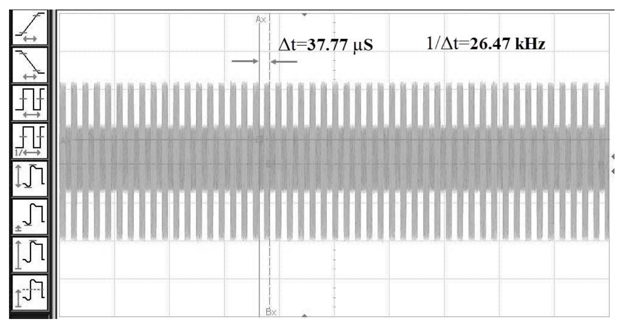

(c)

Fig. 13. Measurement results of reflected signal for chip 1 at (a) at 35°C the output frequency is 2.4 kHz, (b) at 52°C the output frequency is 8.82 kHz and (c) at 70°C the output frequency is 26.47 kHz.

show that as temperature goes up from 35°C to 70°C, the frequency is going up from 2.4 kHz to 26.47 kHz. The measured output reflected signal frequency in response to temperature change for three samples is shown in Fig. 14. As expected, the process variation causes that backscattered frequency for one of the three chips to be significantly different from the other two, further emphasizing the need for the calibration. As can be seen in Fig. 14 and discussed in Section III. B the reflected signal frequency versus temperature has logarithmic behavior. The data can be linearized by calculating the signal response as 10^{E}. Logarithm of reflected signal frequency versus temperature has linear behavior, thus two-point calibration can be done in receiver part for the logarithm of reflected signal frequency with respect to temperature. Therefore, a two-point calibration between the results in Fig. 14 is adopted at 20 °C and 80 °C in receiver part. The reflected signal frequency after calibration and the measured inaccuracy, which represents differences from the fitted lines, are shown in Fig. 15 and Fig. 16, respectively. Within the range of 10°C to 100°C the temperature error is −2.6 to 1.3°C

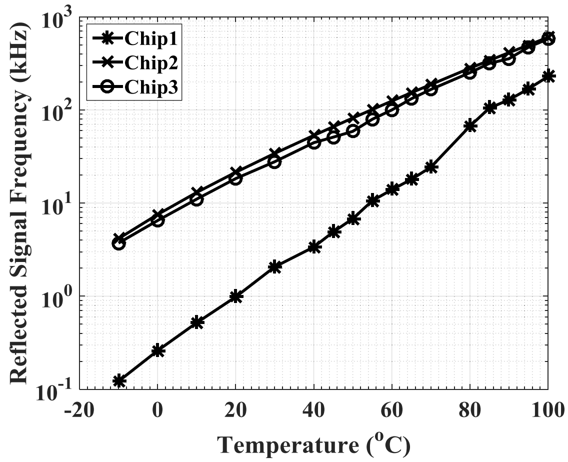

Fig. 14. Measurement of reflected signal frequency versus temperature sweep after calibration for three different chips.

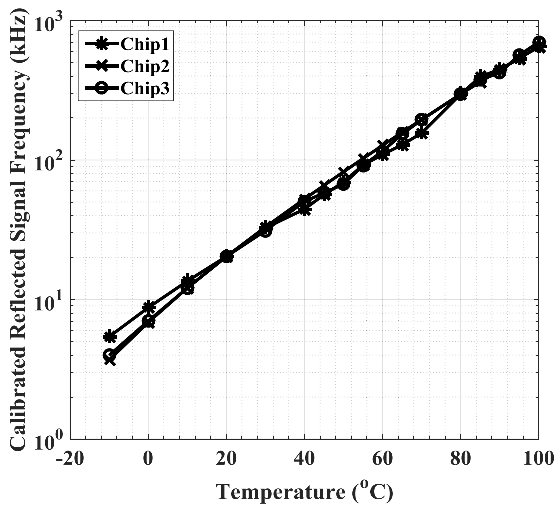

Fig. 15. Measurement of reflected signal frequency versus temperature sweep after calibration for three different chips.

after two-point calibration. Multipoint or nonlinear function fitting can improve the precision, but the complexity will be increased.

It can be seen that frequency is varying exponentially with temperature thus in high temperatures the sensitivity is higher.

From the calibrated data of Fig. 15, it can be seen that between the temperature range of −10°C to -9°C the frequency is changing from 5.321 kHz to 5.559 kHz that is equal to sensitivity of 238Hz/°C. From 26° to 27°C the frequency is changing from 26.57 kHz to 27.784 kHz that gives us the sensitivity of 1.214 kHz/ °C. From 90° to 91 °C the sensitivity is 21.172 kHz/°C and the maximum sensitivity is between 99° to 100° that is 31.648 kHz/°C. The higher sensitivity of sensor in high temperatures makes it suitable for harsh environment monitoring. The sensitivity (Hz/°C) is calculated based on the linear fitting of the measured results taken with the temperature step sizes of 5°C and 10°C.

To highlight the advantage of the proposed work, we can calculate the sensitivity improvement of the oscillation

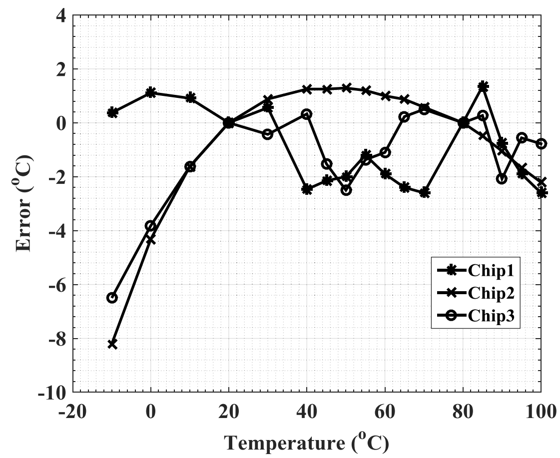

Fig. 16. Measured temperature errors for three chips after two-point calibration at 20°C and 80°C.

frequency to the temperature when using a supply voltage that is varying proportionally with temperature in comparison to using a fixed supply voltage as follows:

$$\text{Sensitivity Improvement } (\%) = \frac{sens(T, V_{\text{var}}(T)) - sens(T, V_{fixed})}{sens(T, V_{fixed})} \times 100, \quad (15)$$

where $V_{\text{var}}(T)$ is equal to temperature-increasing $V_{\text{OUT}-\text{Reg}}$ at temperature of T °C and V_{fixed} is a fixed voltage, and the sensitivity function *sens(T,V)* is defined as

$$sens(T, V(T)) = \frac{Freq(T + \Delta T, V(T + \Delta T)) - Freq(T, V(T))}{\Delta T}, \quad (16)$$

where *Freq(T,V(T))* is the output frequency of ring oscillator at temperature of T °C when it is powered by voltage of V. The sensitivity improvement is plotted in Fig. 17 once based on the above analysis using Equation (15) and another time based on the circuit simulation results. In analytical calculation, the sensitivity is calculated by substituting Equations (2), (3), (6) and (16) in (15) and using the selected values that are chosen for drawing Fig. 5(b) and assuming that $V_{\text{var}}(T)$ is equal to $V_{\text{OUT}-\text{Reg}}$ as shown in Fig. 11, V_{fixed} is equal to $V_{\text{OUT}-\text{Reg}}$ at −10°C (133.9 mV) and ΔT is the steps of 1°C. Fig. 19 shows that the proposed strategy improve the sensitivity 45% at −10°C and more than 500% at temperatures above 70°C.

To verify the proper operation of the sensor with wireless powering, the sensor is powered up wirelessly by connecting the signal generator to the commercial RFID antenna. This antenna transmits the power to the sensor. The second antenna that is connected to the sensor receives the transmitted power to power up the sensor. The sensed temperature is sent back to the first antenna using a frequency-modulated backscattering signal. Wireless test of the chip is performed in room temperature while the device is placed 50 cm away from the transmission antenna with the minimum transmitted power of 10 dBm from the base station. Using Friss' free space propagation formula [36], the power received by the RF-DC converter is calculated to be −15.66 dBm. Fig. 18 shows the

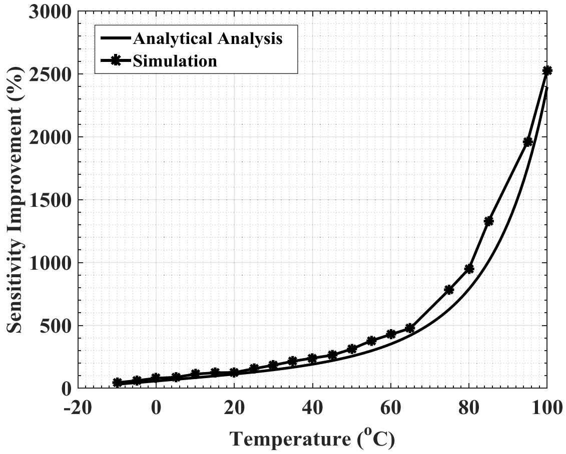

Fig. 17. Sensitivity improvement of proposed work in comparison with using the fixed supply voltage for the ring oscillator temperature sensor.

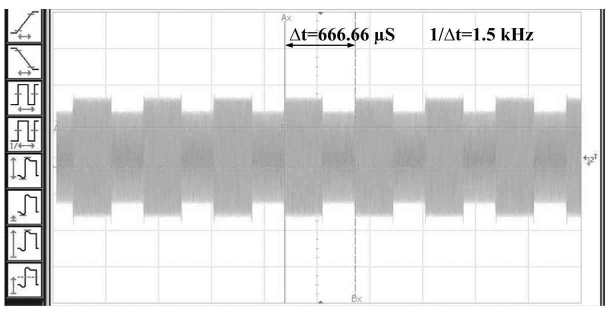

Fig. 18. Measurement results of the reflected signal at room temperature with wireless powering for chip 1.

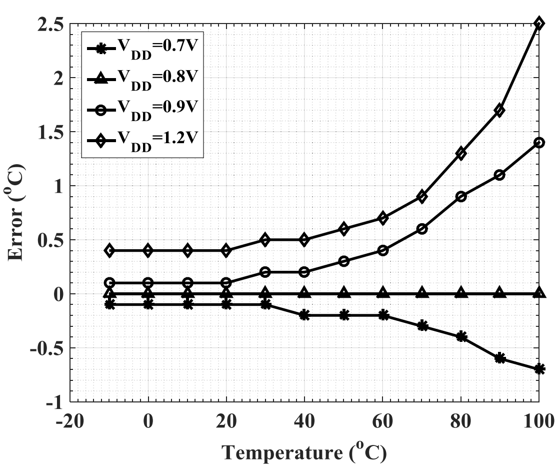

Fig. 19. Inaccuracy of the measured temperature induced by VDD variation for chip 1.

reflected waveform voltage for the chip 1 when the sensor is powered up wirelessly at room temperature.

It can be seen in Fig. 11 that $V_{OUT_{Reg}}$ shifts by a few millivolts when V_{DD} varies between 0.7V and 1.2V. Fig. 19 shows the inaccuracy of the measured temperature induced by variation of the V_{DD}. For temperatures below 60°C, the inaccuracy due to V_{DD} variation is below 1°C.

Fig. 20 shows the total power consumption of the sensor and its building blocks as functions of the temperature. The voltage limiter, level shifter and buffer, and temperature

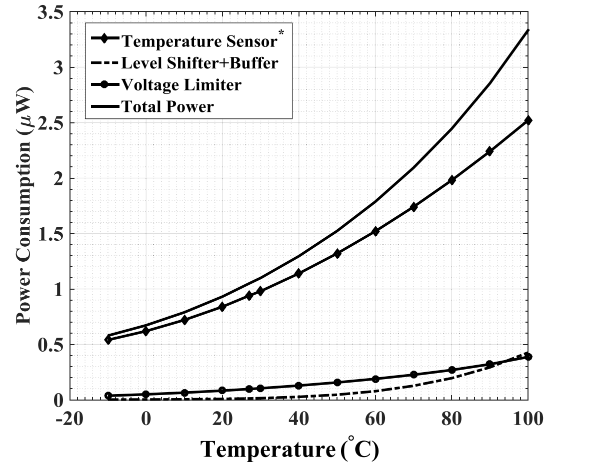

*Temperature Sensor = Voltage regulator with embedded voltage reference + Ring oscillator temperature sensor.

Fig. 20. Measured power consumption versus temperature.

TABLE I

POWER AND AREA BREAKDOWN OF THE SYSTEM

	Area (mm^2)	Power Consumption (µW) at Room temperature (27°C)
RF-DC Converter	0.14	-
Voltage Limiter	0.0011	0.0976
Voltage Regulator	0.01	0.94
Ring Oscillator	0.016	0.001
Level Shifter + Buffer	0.006	0.015
Total System	0.23	1.05

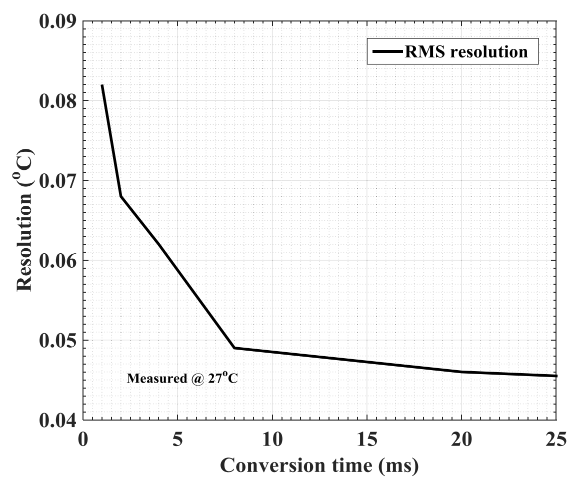

Fig. 21. RMS resolution versus conversion time at 27°C.

sensor (voltage regulator and oscillator) consume 9.2%, 1.4%, 89.4% of the total power at room temperature of 27°C, respectively, and 11.1%, 13%, 75.9% of the total power at 100°C, respectively. The total power consumption of the sensor at room temperature is about 1.05 uW increasing to 3.35 uW at 100°C. Table I summarizes the room-temperature power consumptions and the chip areas of each block of the entire system.

RMS resolution of the proposed sensor is plotted in Fig. 21. After 25 ms of conversion time, a resolution of 0.046°C is obtained at 27°C. Because of the exponential frequency-temperature relation in the proposed temperature sensor, this

TABLE II
PERFORMANCE SUMMARY AND COMPARISON

	[3]	[37]	[38]	[39]	[40]	This work
Temperature Sensor	CMOS	BJT	SAW resonator	CMOS	CMOS	CMOS
Circuit Technology	0.25-μm CMOS	0.18-μm CMOS	0.18-μm/65-nm CMOS	0.18-μm CMOS	65-nm CMOS	0.13-μm CMOS
Chip Area	1.2 mm^2	1.2 mm^2	0.112 mm^2 ***	0.09mm^2	0.008mm^2	0.23 mm^2
Wirelessly Powered	YES	YES	YES	NO	NO	YES
Incident Signal Frequency	450 MHz	915 MHz	-	-	-	915 MHz
Wireless Sensitivity	-12.3 dBm	-5 dBm	-	-	-	-16 dBm
Energy Source	RF	RF	Vibration	-	-	RF
Temperature Range	-40° C-40° C	-35° C-105° C	-40° C-120° C	0-100°C	0-110°C	10° C-100° C
Temperature Accuracy	-	-1.9° C ~ 2.3° C	±0.6° C	-1.4°C~1.5°C	-1.5°C~1.5°C	-2.6° C ~ 1.3° C
Active Power Consumption	1.7 mW *	12.8 μW	61.5 μW	71 nW	500 μW	1.05 μW
Resolution	-	0.31°/LSB	-	0.3°C	0.94°C	0.046°C
Conversion time	-	2ms	-	30ms	0.00213ms	25ms
Operation Distance	18.3 m**	-	-	-	-	10.4 m****
Calibration	-	-	-	Two-Point	One-Point	Two-Point

* Estimated from voltage and current consumption, **predicted operation distance with 7W incident power, *** Estimated area of two chips without including off-chip SAW resonator, **** predicted operation distance with 4W incident power.

system exhibits good resolution as other non-ideal noise exhibits linear behavior [34].

This designed circuit is predicted to work in maximum range of 10.4m with a 4-W base transmit power. A summary of overall sensor specifications and comparison with other state-of-art wireless temperature sensors are given in Table II including three sensors [3], [37], and [38] that are wirelessly powered and two sensors [39] and [40] without wireless powering. Among the wirelessly-powered sensors, our proposed sensor achieves the lowest chip area except for [38] that uses an off-chip temperature sensor. The proposed sensor requires the minimum amount of power (−16 dBm) to operate among all reported wirelessly power sensors. The power consumption is also the lowest among the reported works except for [39] that is a sensor without RF energy harvester, regulator, and backscattering switch. Finally the proposed sensor achieves the highest resolution among the reported sensors while its slightly higher inaccuracy is caused by extra temperature sensitivity and slight variations of voltages supplied by the regulator at high temperatures.

V. CONCLUSION

In this paper, we reported the design and implementation of an RF-powered wireless temperature sensor that can operate non-intermittently, backscattering the sensed temperature to an external reader. To achieve a minimalistic design to minimize the power consumption and cost, a sub-threshold ring oscillator is used to both sense the temperature and produce a frequency-modulated backscattered signal for wireless transmission. For the sensor to operate properly, a novel voltage regulator is developed that produces a relatively constant output voltage as the supply voltage of the ring oscillator for a large range of harvested input energy but allow the output voltage to change as a function of the temperature for added temperature sensitivity of the overall sensor. Fabricated in IBM's 130 nm CMOS process, the measured power consumption of the entire sensor system is 1.05 μW at room temperature. The sensor was tested between −10° to 100°C exhibiting a minimum sensitivity of 238Hz/°C at −10°C and a maximum sensitivity of 31.648kHz/°C at 100°C. The maximum wireless operation range is measured to be 50 cm when it is powered using a commercial RFID tag antenna with a transmitted power of 10 dBm that can be extended even further with high gain antennas and higher input power. The predicted temperature error is −2.6 to 1.3°C using a two-point calibration within the range of 10°C to 100°C. The temperature sensor exhibits a resolution of 0.046°C (rms) with a conversion time of 25 ms at 27°C.

ACKNOWLEDGMENT

The authors would like to thank the Canadian Microelectronics Corporation (CMC) for providing design tools and fabrication support.

REFERENCES

[1] Y. K. Tan, *Energy Harvesting Autonomous Sensor Systems: Design, Analysis, and Practical Implementation*. Boca Raton, FL, USA: CRC Press, 2013.

[2] J. Olivo, S. Carrara, and G. De Micheli, "Energy harvesting and remote powering for implantable biosensors," *IEEE Sensors J.*, vol. 11, no. 7, pp. 1573–1586, Jul. 2011.

[3] F. Kocer and M. P. Flynn, "An RF-powered, wireless CMOS temperature sensor," *IEEE Sensors J.*, vol. 6, no. 3, pp. 557–564, Jun. 2006.

[4] H. Reinisch *et al.*, "An electro-magnetic energy harvesting system with 190 nW idle mode power consumption for a BAW based wireless sensor node," *IEEE J. Solid-State Circuits*, vol. 46, no. 7, pp. 1728–1741, Jul. 2011.

[5] Y. Zhang *et al.*, "A batteryless 19 μW MICS/ISM-band energy harvesting body sensor node SoC for ExG applications," *IEEE J. Solid-State Circuits*, vol. 48, no. 1, pp. 199–213, Jan. 2013.

[6] L. Xia, J. Cheng, N. E. Glover, and P. Chiang, "0.56 V, –20 dBm RF-powered, multi-node wireless body area network system-on-a-chip with harvesting-efficiency tracking loop," *IEEE J. Solid-State Circuits*, vol. 49, no. 6, pp. 1345–1355, Jun. 2014.

[7] G. C. Martins and F. R. de Sousa, "An RF-powered temperature sensor designed for biomedical applications," in *Proc. IEEE Integr. Circuits Syst. Design*, Curitiba, Brazil, Sep. 2013, pp. 1–6.
[8] H. Jabbar, Y. S. Song, and T. T. Jeong, "RF energy harvesting system and circuits for charging of mobile devices," *IEEE Trans. Consum. Electron.*, vol. 56, no. 1, pp. 247–253, Feb. 2010.
[9] *FCC Codes of Regulation*. Accessed: Oct. 2016. [Online]. Available: http://www.access.gpo.gov/nara/cfr/waisidx_03/47cfr15_03.htmpt.15
[10] G. Papotto, F. Carrara, A. Finocchiaro, and G. Palmisano, "A 90-nm CMOS 5-Mbps crystal-less RF-powered transceiver for wireless sensor network nodes," *IEEE J. Solid-State Circuits*, vol. 49, no. 2, pp. 335–346, Feb. 2014.
[11] L. Magnelli, F. Crupi, P. Corsonello, C. Pace, and G. Iannaccone, "A 2.6 nW, 0.45 V temperature-compensated subthreshold CMOS voltage reference," *IEEE J. Solid-State Circuits*, vol. 46, no. 2, pp. 465–474, Feb. 2011.
[12] A. Wang and A. Chandrakasan, "A 180-mV subthreshold FFT processor using a minimum energy design methodology," *IEEE J. Solid-State Circuits*, vol. 40, no. 1, pp. 310–319, Jan. 2005.
[13] D. Liu and C. Svensson, "Trading speed for low power by choice of supply and threshold voltages," *IEEE J. Solid-State Circuits*, vol. 28, no. 1, pp. 10–17, Jan. 1993.
[14] S. Park, C. Min, and S. H. Cho, "A 95 nW ring oscillator-based temperature sensor for RFID tags in 0.13 μm CMOS," in *Proc. IEEE Int. Symp. Circuits Syst. Conf.*, May 2009, pp. 1153–1156.
[15] G. Popov, F. C. Dualibe, V. Moeyaert, P. Ndungidi, H. García-Vázquez, and C. Valderrama, "A 65-nm CMOS battery-less temperature sensor node for RF-powered wireless sensor networks," in *Proc. IEEE Wireless Power Transf. Conf.*, Aveiro Municipality, Portugal, May 2016, pp. 1–4.
[16] H. Reinisch *et al.*, "A multifrequency passive sensing tag with on-chip temperature sensor and off-chip sensor interface using EPC HF and UHF RFID technology," *IEEE J. Solid-State Circuits*, vol. 46, no. 12, pp. 3075–3088, Dec. 2011.
[17] A. Vaz *et al.*, "Full passive UHF tag with a temperature sensor suitable for human body temperature monitoring," *IEEE Trans. Circuits Syst. II, Exp. Briefs*, vol. 57, no. 2, pp. 95–99, Feb. 2010.
[18] H. Nakamoto *et al.*, "A passive UHF RF identification CMOS tag IC using ferroelectric RAM in 0.35-μm technology," *IEEE J. Solid-State Circuits*, vol. 42, no. 1, pp. 101–110, Jan. 2007.
[19] T. Le, K. Mayaram, and T. Fiez, "Efficient far-field radio frequency energy harvesting for passively powered sensor networks," *IEEE J. Solid-State Circuits*, vol. 43, no. 5, pp. 1287–1302, May 2008.
[20] G. Papotto, F. Carrara, and G. Palmisano, "A 90-nm CMOS threshold-compensated RF energy harvester," *IEEE J. Solid-State Circuits*, vol. 46, no. 9, pp. 1985–1997, Sep. 2011.
[21] Z. Hameed and K. Moez, "Fully-integrated passive threshold-compensated PMOS rectifier for RF energy harvesting," in *Proc. IEEE 56th Int. Midwest Symp. Circuits Syst.*, Aug. 2013, pp. 129–132.
[22] Z. Hameed and K. Moez, "Hybrid forward and backward threshold-compensated RF-DC power converter for RF energy harvesting," *IEEE J. Emerg. Sel. Topics Circuits Syst*, vol. 4, no. 3, pp. 335–343, Sep. 2014.
[23] Z. Hameed and K. Moez, "A 3.2 V –15 dBm adaptive threshold-voltage compensated RF energy harvester in 130 nm CMOS," *IEEE Trans. Circuits Syst. I, Reg. Papers*, vol. 62, no. 4, pp. 948–956, Apr. 2015.
[24] A. Shrivastava, N. E. Roberts, O. U. Khan, D. D. Wentzloff, and B. H. Calhoun, "A 10 mV-input boost converter with inductor peak current control and zero detection for thermoelectric and solar energy harvesting with 220 mV cold-start and −14.5 dBm, 915 MHz RF kick-start," *IEEE J. Solid-State Circuits*, vol. 50, no. 8, pp. 1820–1832, Aug. 2015.
[25] P.-H. Hsieh, C. H. Chou, and T. Chiang, "An RF energy harvester with 44.1% PCE at input available power of −12 dBm," *IEEE Trans. Circuits Syst. I, Reg. Papers*, vol. 62, no. 6, pp. 1528–1537, Jun. 2015.
[26] M. A. Abouzied, K. Ravichandran, and E. Sánchez-Sinencio, "A fully integrated reconfigurable self-startup RF energy-harvesting system with storage capability," *IEEE J. Solid-State Circuits*, vol. 52, no. 3, pp. 704–719, Mar. 2017.
[27] J. F. Dickson, "On-chip high-voltage generation in MNOS integrated circuits using an improved voltage multiplier technique," *IEEE J. Solid-State Circuits*, vol. 11, no. 3, pp. 374–378, Jun. 1976.
[28] U. Kaiser and W. Steinhagen, "A low-power transponder IC for high-performance identification systems," *IEEE J. Solid-State Circuits*, vol. 30, no. 3, pp. 306–310, Mar. 1995.
[29] W.-C. Chen, Y.-P. Su, Y.-H. Lee, C.-L. Wey, and K.-H. Chen, "0.65 V-input-voltage 0.6 V-output-voltage 30 ppm/°C low-dropout regulator with embedded voltage reference for low-power biomedical systems," in *IEEE Int. Solid-State Circuits Conf. (ISSCC) Dig. Tech. Papers*, Feb. 2014, pp. 304–305.
[30] J. Guo and K. N. Leung, "A 6-μ W chip-area-efficient output-capacitorless LDO in 90-nm CMOS technology," *IEEE J. Solid-State Circuits*, vol. 45, no. 9, pp. 1896–1905, Sep. 2010.
[31] Y. Taur and T. H. Ning, *Fundamentals of Modern VLSI Devices*. Cambridge, U.K.: Cambridge Univ. Press, 1998.
[32] P. E. Allen and D. R. Holberg, *CMOS Analog Circuit Design*. Oxford, U.K.: Oxford Univ. Press, 2002.
[33] E. Socher, S. M. Beer, and Y. Nemirovsky, "Temperature sensitivity of SOI-CMOS transistors for use in uncooled thermal sensing," *IEEE Trans. Electron Devices*, vol. 52, no. 12, pp. 2784–2790, Dec. 2005.
[34] K. Yang *et al.*, "9.2 A 0.6nJ $-0.22/+0.19$ °C inaccuracy temperature sensor using exponential subthreshold oscillation dependence," in *IEEE Int. Solid-State Circuits Conf. (ISSCC) Dig. Tech. Papers*, Feb. 2017, pp. 160–161.
[35] S.-C. Luo, C.-J. Huang, and Y.-H. Chu, "A wide-range level shifter using a modified Wilson current mirror hybrid buffer," *IEEE Trans. Circuits Syst. I, Reg. Papers*, vol. 61, no. 6, pp. 1656–1665, Jun. 2014.
[36] D. K. Cheng, *Field and Wave Electromagnetics*. Reading, MA, USA: Addison-Wesley, 1989.
[37] J. Qian *et al.*, "A passive UHF tag for RFID-based train axle temperature measurement system," in *Proc. IEEE Custom Integr. Circuits Conf.*, San Jose, CA, USA, Sep. 2011, pp. 1–4.
[38] Y. Zhu *et al.*, "An energy autonomous 400 MHz active wireless SAW temperature sensor powered by vibration energy harvesting," *IEEE Trans. Circuits Syst. I, Reg. Papers*, vol. 62, no. 4, pp. 976–985, Apr. 2015.
[39] S. Jeong, Z. Foo, Y. Lee, J.-Y. Sim, D. Blaauw, and D. Sylvester, "A fully-integrated 71 nW CMOS temperature sensor for low power wireless sensor nodes," *IEEE J. Solid-State Circuits*, vol. 49, no. 8, pp. 1682–1693, Aug. 2014.
[40] S. Hwang, J. Koo, K. Kim, H. Lee, and C. Kim, "A 0.008 mm^2 500 μW 469 kS/s frequency-to-digital converter based CMOS temperature sensor with process variation compensation," *IEEE Trans. Circuits Syst. I, Reg. Papers*, vol. 60, no. 9, pp. 2241–2248, Sep. 2013.

Parvaneh Saffari (S'15) received the B.Sc. and M.Sc. degrees (Hons.) in electrical engineering from the Ferdowsi University of Mashhad, Mashhad, Iran, in 2010 and 2013, respectively. She is currently pursuing the Ph.D. degree with the Integrated Circuits and Systems Laboratory, Department of Electrical Engineering, University of Alberta, Edmonton, AB, Canada.

Her current research interests are on integrated RF energy harvesting systems, low power low-voltage analog and mixed-signal integrated circuits design, and RFIC.

Ali Basaligheh (S'15) is currently pursuing the Ph.D. degree in electrical engineering with the Integrated Circuits and Systems Laboratory, Department of Electrical Engineering, University of Alberta, Edmonton, AB, Canada.

From 2009 to 2011, he was a Researcher with the Electrical Engineering Department, Sharif University of Technology, Tehran, Iran. In 2011, he joined the Sun and Air Research Institute, Ferdowsi University of Mashhad, Mashhad, Iran, where he worked in the design of power amplifiers in GaN and CMOS technologies. He was a Research Assistant with the ECE Department, University of Concordia, Montreal, QC, Canada, in 2014, where he was involved in the modeling of inductive proximity sensors for the THALES group. In 2015, he joined as an RFIC Packaging Researcher with the institutional Research Centre on the Co-Design and Fabrication of Microsystems Laboratory, University of Quebec, Montreal, QC, Canada. In 2015, he collaborated with the University of Alberta, where he was involved in design of RF-powered wireless temperature sensor.

His research interests include millimeter-wave and sub-THz integrated circuit design for wireless communications.

Vincent J. Sieben received the Ph.D. degree from the Department of Electrical and Computer Engineering, University of Alberta, in 2008. From 2008 to 2011, he conducted pioneering research on subsea microfluidic systems for measuring nutrients and microbiology while at the National Oceanography Center, Southampton, U.K. He joined Schlumberger in 2011. He is currently at the Schlumberger-Doll Research, Cambridge, MA, USA, as a Senior Research Scientist. He was the Lead Scientist of Maze microfluidic SARA. His current research activities encompass the areas of microfabrication and photonics for enabling novel fluid analysis instrumentation.

Kambiz Moez (S'01–M'07–SM'12) received the B.Sc. degree in electrical engineering from the University of Tehran, Tehran, Iran, in 1999, and the M.Sc. and Ph.D. degrees from the University of Waterloo, Waterloo, ON, Canada, in 2002 and 2006, respectively. Since 2007, he has been with the Department of Electrical and Computer Engineering, University of Alberta, Edmonton, AB, Canada, where he is currently an Associate Professor. His current research interests include the analysis and design of radio frequency CMOS integrated circuits and systems for variety of applications including wired/wireless communications, biomedical imaging, instrumentations, and radars. He is a registered Professional Engineer in Alberta.